12

Optical Properties of Molecular Crystals: The Effect of Molecular Packing and Polymorphism

Silvia Tavazzi[1], Leonardo Silvestri[2] and Peter Spearman[1]
[1]*University of Milano Bicocca, Materials Science Department,*
[2]*School of EE&T, University of New South Wales,*
[1]*Italy*
[2]*Australia*

1. Introduction

Modern technologies rely not only on traditional inorganic semiconductors, but also on organic materials. In particular, organic semiconductors based on conjugated oligomers and polymers have technological applications owing to their compatibility with low-temperature processing, the relatively simple thin-film device fabrication, and the tunability of their electronic properties based on the richness of synthetic organic chemistry. Here, we are interested in molecular materials in their crystalline form, which play a role in the fields of both theoretical and experimental research. We will focus the attention on their UV-visible optical properties.

Compared to amorphous films, crystalline materials exhibit well defined polarization of the electronic states and interesting effects related to the anisotropic propagation of light. First of all, in order to maximize coupling to the crystal electronic transition moment, the pumping photon beams must be precisely aligned (Fichou et al. 1997). Emission is then observed with defined directions of propagation and of polarization. Optical gain can also result in amplified spontaneous emission (ASE), which is characterized by a spectrally narrowed emission upon increasing the excitation fluence above a threshold. Gain-narrowing has been demonstrated in a number of molecular crystalline materials, such as oligothiophenes, oligo(p-phenylene), oligo(p-phenylene vinylene), trans-1,4-distyrylbenzene, cyano derivatives, fluorene/phenylene co-oligomers, hydroxy-substituted tetraphenyl-imidazole, and 1,1,4,4-tetraphenyl-1,3-butadiene (Fichou et al. 1997, 1999; Hibino et al. 2002; Horowitz et al. 1999; Ichikawa et al. 2003, 2005; Losio et al. 2007; Nagawa et al. 2002; Park et al. 2005; Polo et al. 2008; Tavazzi et al. 2006c, 2007, 2008, 2010b; Xie et al. 2007; Zhu et al. 2003). Relatively low thresholds have been recently reported for p-sexiphenyl samples. Self-waveguided emission has been observed in needle-shaped crystals of this molecular species grown on potassium chloride (001) substrates (Cordella et al. 2007; Quochi et al. 2005; Yanagi et al. 2001; Yanagi & Morikawa 1999) with threshold down to 0.5 μJ/cm^2. Random lasing from isolated nanofibres of various widths has also been reported and discussed by Quochi et al. (Quochi et al. 2005). For the same molecular species in the bulk crystalline form, ASE was reported (Losio et al. 2007) with different thresholds depending on the

pumping rates (ns: 0.885 mJ/cm², fs: 0.110 mJ/cm²). The same authors also reported that exciton annihilation seems to be responsible for the increase of the ASE threshold in bulk crystals compared to nanofibers. The increase was attributed to differences in the exciton annihilation rate from the nanofibres to crystals, which, in turn, were attributed to the different molecular packing, namely to the different crystalline phase of bulk crystals with respect to nanofibres. Another example of emission gain narrowing has been reported to occur for single crystals of a thiophene/phenylene co-oligomer (Ichikawa et al. 2003; Nagawa et al. 2002). For these co-oligomers, thresholds as low as 0.027 mJ/cm² at room temperature have also been reported. Besides ASE and random lasing, some studies have also been reported on the coupling of excitons with photons in microcavity structures – which is a rapidly growing field of research, in particular as far as strong coupling phenomena are concerned, which may lead to novel laser devices such as the *polariton laser* (Klaers et al. 2010). Strong exciton-photon coupling has been demonstrated in microcavities of single crystal and thin film anthracene (Kena-Cohen et al. 2008; Kondo et al. 2009, 2008). More recently, Kéna-Cohen and Forrest observed polariton lasing at room temperature from a microcavity containing melt-grown anthracene single-crystal, with a threshold lower than the estimated threshold for conventional lasing in the same system (Kéna-Cohen et al. 2010). In order to better understand the origin of some gain-narrowed emission bands of molecular single crystals, the dependence of the excitation threshold on excitation lengths has been studied for poly(p-phenylene-vinylene) (Frolov et al. 1998) and for 5,5′′-bis(4-biphenylyl)-2,2′:5′,2′′-terthiophene (Hiramatsu et al. 2009; Matsuoka et al. 2010).

Here, we discuss three prototypical molecular crystals. They show remarkable changes in the energy, intensity, order, and polarization of the optical bands with respect to the single molecule. These species are: (i) 1,1,4,4-tetraphenyl-1,3-butadiene (TPB), a highly-efficient blue emitting material, (ii) dibenzo[d,d′]thieno[3,2-b;4,5-b′]dithiophene (DBTDT), a stable heteroacene reported in the literature for its good field effect mobility, (iii) N-pyrrole end-capped thiophene/phenyl co-oligomer (TPP), a molecule designed to explore the effect of an electron-rich aromatic ring, such as pyrrole, to end-cap oligothiophenes. Fig. 1 shows the structure of the three selected molecular species. TPB is taken into consideration to discuss possible remarkable differences between polymorphs of the same molecular species.

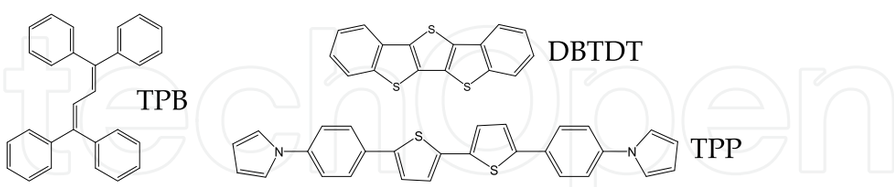

Fig. 1. Molecular structures of 1,1,4,4-tetraphenyl-1,3-butadiene (TPB), dibenzo[d,d′]thieno[3,2-b;4,5-b′]dithiophene (DBTDT), N-pyrrole end-capped thiophene/phenyl co-oligomer (TPP).

DBTDT is used as example to discuss the possible changes of the order of the excited states due to intermolecular interactions. Finally, TPP offers a prime example of the phenomenon of directional dispersion in which the molecular orientation within the crystal exposed face affects the absorption spectra. The chapter discusses some different techniques for the growth of molecular crystals (Section 2) and the microscopic and macroscopic theories of their optical properties, which is applied to the three selected species (Section 3). The general

focus is on the UV-visible absorption properties, which are described and rationalised in the framework of the exciton theory of molecular materials. Some discussion on the emission properties is also given, but on a more qualitative level related to the molecular organization within the crystal. We emphasise that for a full description of the polarized emission spectra of molecular crystals, the excitonic bands should be studied as a function of momentum in the first Brillouin zone, while these details are here omitted. In contrast, for the interpretation of the absorption properties only the excitons at the centre of the Brillouin zone (k=0) need to be considered.

2. Growth of molecular crystals

2.1 Vapour-transport growth

The physical vapour growth of organic semiconductors is well described in the literature (Kloc et al. 1997; Kloc & Laudise 1998; Laudise et al. 1998; Siegrist et al. 1998). We have adopted a horizontal reactor arrangement, similar in design to that described by Laudise et al. (Laudise et al. 1998). The tube was placed in a three-zone furnace, which provided a suitable temperature gradient along the length of the tube under inert gas (nitrogen) at a flow rate of the order of a few tens of ml/min. The starting material was placed in a glass crucible at the position of the source temperature. For example, for the growth of TPB crystals the source was heated at 175°C in the first zone. The temperature descended to 135° at the end zone following a roughly linear temperature gradient. The nitrogen flux was 50 ml/min. Platelet crystals were obtained; few images are shown taken under the optical microscope (Fig. 2) and under the fluorescence microscope (Fig. 3).

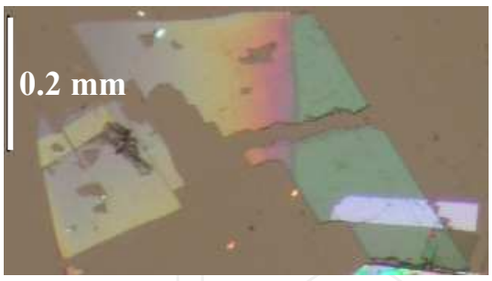

Fig. 2. Image under the optical microscope of α-TPB crystals grown by the vapour transport method. It was taken with polarizer and analyser parallel to each other and to a crystal principal axis. Coloured fringes are interference fringes in regions of different thickness.

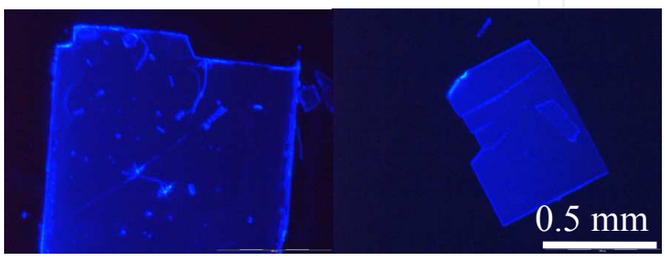

Fig. 3. Image under the fluorescence microscope of TPB crystals grown by the vapour-transport method.

2.2 Floating-drop growth

An alternative method for the growth of molecular crystals uses the technique of mixed solvents with different solubility in the extreme case where the molecule is completely insoluble in one of the solvents. The level of supersaturation in solution is typically lower than that of the vapour phase, so that the nucleation rate is reduced and the size of the crystal typically increases. To further reduce the nucleation, often induced by the vessel walls, the solution can be left on the surface of a denser and immiscible liquid. This method has been described elsewhere and called floating-drop technique (Adachi et al. 2003; Campione et al. 2005). For example, single crystals of DBTDT were obtained by such a floating-drop technique. Crystals grew as platelets with one accessible face for optical investigation. Images of a crystal are reported in Fig. 4 as taken under the optical microscope. The image on the left was taken with crossed polarizer and analyzer for a generic orientation of the sample. In this configuration, the emerging electric field is rotated with respect to the incident electric field and the angle of rotation depends on the wavelength of light and on the crystal thickness (birefringence). For this reason, the crystal is clearly distinguishable with respect to the dark background. The image on the right was taken with parallel polarizer and analyzer. The crystal appears slightly coloured (yellow due to the absorption of the complementary blue light).

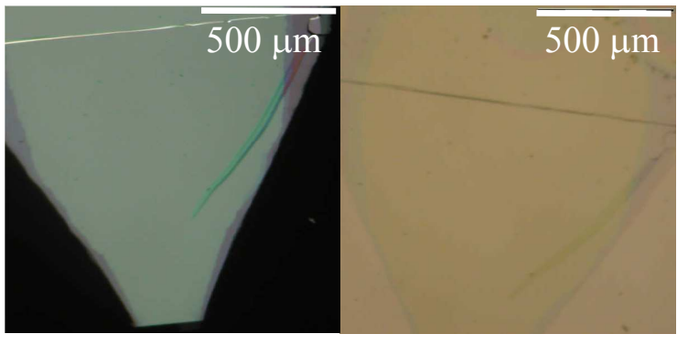

Fig. 4. Images of a DBTDT crystal grown by the floating-drop technique taken under the optical microscope with either crossed (left) or parallel (right) polarizer and analyzer.

2.3 Melt growth

When a molecular species possesses a well-defined melting point and remains stable at the corresponding temperature, crystals can be grown from the melted compound. This method is useful for incorporating crystalline materials into well-defined device geometries and several examples have been reported in the literature. For example, Hibino and co-workers reported the crystallization from the melt of anthracene and other oligomers (Hibino et al. 2002). They also observed ASE for many of them. The technique has also been adopted by Forrest's group in the fabrication of organic crystalline microcavities of anthracene grown by the melted compound (Kena-Cohen et al. 2008, Kena-Cohen et al. 2010). Another example has been reported (Liu & Bard 2000) on the growth and purification by zone-melting of organic single-crystals. Our group has similarly employed the melt-growth technique to grow crystals of the compounds TPB and TPP. Figure 5 displays an image taken under an optical microscope of a TPB crystal grown from the melted compound onto a quartz substrate. This substrate was initially functionalized with trichloro 3-bromopropylsilane followed by bromine substitution with dithiocarbamate. Large crystalline domains are

observed. Other images of TPB grown from the melt between two quartz substrates are shown in Fig. 6. In this case, a fan-like distribution originating form a nucleation point is observed. The alternating ridge and valley bands are indicative of a rhythmic type of crystal growth as a result of the inability of the molten TPB to diffuse to the crystallization front. The image on the left (right) was taken with parallel (crossed) polarizer and analyzer.

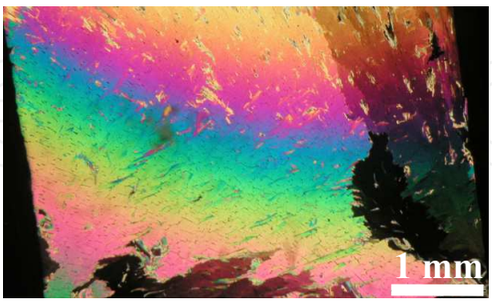

Fig. 5. Image taken under the optical microscope of TPB grown from the melted compound on a functionalized quartz substrate. The image was taken with crossed polarizer and analyzer for a generic orientation of the crystal, so that both interference and birefringence (but manly birefringence) contribute to give the observed fringes in regions of different thickness.

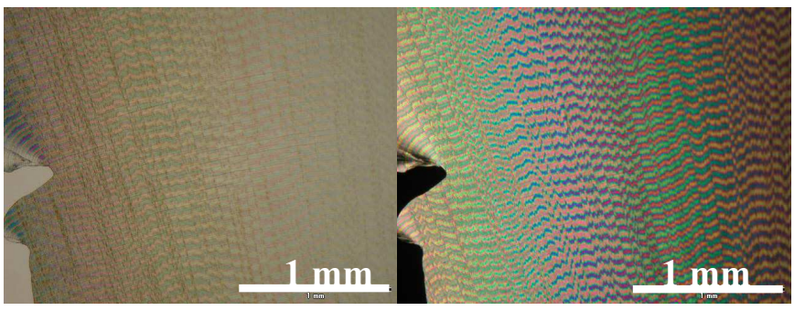

Fig. 6. Images under the optical microscope of a melt-grown TPB sample. They were taken with either parallel (left) or crossed (right) polarizer and analyzer for a generic orientation of the sample. Both interference and birefringence contribute to give the coloured fringes in regions of different thickness.

Another compound that is suitable for melt growth is TPP. Figure 7 shows the images taken under the fluorescence microscope at different temperatures during the growth of a sample of TPP from the melted compound. The starting polycrystalline powder was placed in the hot-stage apparatus and heated. The starting polycrystalline powder shows a disordered orange photoluminescence (inset of the first panel). The emission colour shifts to the green where the melting point (T=380°C) is approached (panel 1). Upon decreasing the temperature, crystallization takes place and abruptly the green regions clearly show orange borders and dark exposed surface (panels 2 and 3), which are even more evident when further decreasing the temperature (panel 4). We mention that a discrepancy between the nominal temperatures and the temperature of the sample is expected due to the presence of a quartz substrate between the material and the heating element.

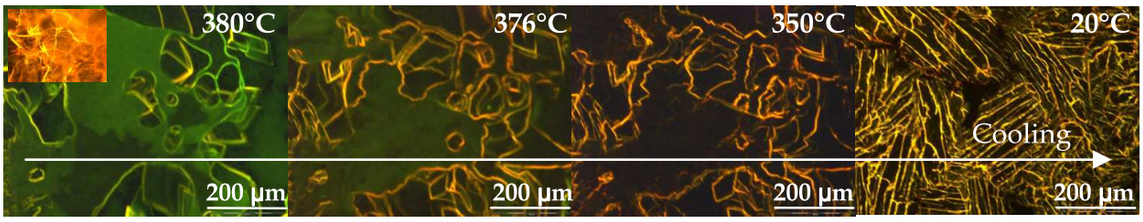

Fig. 7. Images under the fluorescence microscope of a sample of TPP grown from the melted material. Inset: starting polycrystalline powder.

Figure 8 shows a fluorescence microscope image of another melt-grown TPP crystal. The macroscopic order and the presence of cracks in this type of crystal are likely to be improved by adopting a slower and proper temperature profile during the growth. Nevertheless, these crystals exhibit self-waveguiding of the emitted light as a consequence of molecular packing and the melt technique is highly suited as a possible approach for device integration.

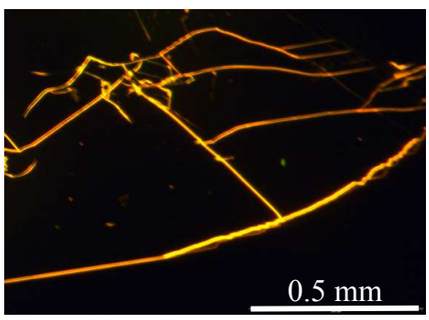

Fig. 8. Fluorescence microscope image of a crystal of TPP.

3. UV-visible optical properties of molecular crystals

3.1 Microscopic and macroscopic theory of the optical properties of molecular crystals

Organic molecular semiconductors are formed by molecules interacting via relatively weak van der Waals forces. Parallel molecular stacking, herringbone, and face-to-face arrangements are often found in the solid state. Absorption and emission spectra of molecular crystals are dominated by Frenkel excitons, which are very different from the Wannier-Mott excitons of conventional inorganic semiconductors. Molecular crystals are characterized by electronic energy bands separated by energy gaps. However, the band gap is strongly influenced by the molecular electronic transition between the highest occupied molecular orbital (HOMO) and the lowest unoccupied molecular orbital (LUMO) and it can be easily tuned to cover the whole UV-visible range by selecting the appropriate organic molecule. Molecular crystals are also characterized by narrow bands as a function of momentum **k** (typical bandwidths of tenths of an electronvolt), relatively large effective masses, and small dielectric constants. Due to these structural properties, they support Frenkel excitons, which consist of electron-hole pairs residing on the same molecule and have large binding energies (of the order of 1 eV). In addition, excitonic transitions in these materials typically show strong optical anisotropy, often associated with strong directional dispersion depending on the direction of the incoming light. By contrast, inorganic semiconductors, which are made of covalently bonded atoms, have relatively wide bands,

small effective masses, and large dielectric constants. They therefore support Wannier-Mott excitons, characterized by a large electron-hole separation (much larger than the lattice constant) and by a small binding energy (of the order of 1 meV). Another striking difference between the two classes of semiconductors is that an optical excitation can easily create Frenkel excitons in molecular crystals, while it usually creates free carriers in inorganic semiconductors, Wannier-Mott exciton absorption lines appearing only at low temperatures just below the band edge.

In the following, we discuss the role that molecular packing plays in governing the UV-visible optical properties of molecular materials. In the framework of the Frenkel-Davydov theory, molecules in a crystal are treated as two level systems where the excited state corresponds to the presence of a Frenkel exciton. When interactions between different molecules are taken into account, optical properties are determined by the eigenstates of the whole crystal and they strongly depend on molecular packing. Since intermolecular interactions are much smaller than the molecular transition energy, coupling between crystal states with different numbers of excitons can be neglected. This is called the Heitler-London approximation. In the materials we study, molecular excitations occur in the UV-visible range of the spectrum and optical properties are mainly determined by crystal states with a single exciton. Within the above approximations we will now consider a molecular crystal made of N cells, each containing σ molecules. Crystal excitonic states are conveniently expressed in terms of delocalized states with a given wave vector **k**, defined as

$$\left|\mathbf{k},\alpha\right\rangle = N^{-1/2}\sum_{\mathbf{n}}\exp\left(i\mathbf{kn}\right)\left|\mathbf{n},\alpha\right\rangle,$$

where

$$\left|\mathbf{n},\alpha\right\rangle$$

indicates a state in which the electronic excitation resides on molecule α in cell **n** while all other molecules in the crystal are in their ground state. The σ excitonic bands at each **k** can then be found by diagonalizing the crystal Hamiltonian

$$H = \hbar\omega_0 + D + \sum_{\mathbf{k},\alpha,\beta}\tilde{J}_{\alpha\beta}(\mathbf{k})\left|\mathbf{k},\alpha\right\rangle\left\langle\mathbf{k},\beta\right| \quad (1)$$

where $\hbar\omega_0$ is the molecular excitation energy, D is the gas-to-crystal shift and the resonance-interaction matrix is defined as

$$\tilde{J}_{\alpha\beta}(\mathbf{k}) = \sum_{\mathbf{n}}{}'\exp\left(i\mathbf{kn}\right)J_{\alpha\beta}(\mathbf{n}) \quad (2)$$

$J_{\alpha\beta}(\mathbf{n})$ being the interaction energy between a molecule of type α in cell **0**=(0, 0, 0) and a molecule of type β in cell **n**. The primed summation indicates that self-interaction must be excluded, i.e. if α=β then **n**≠(0, 0, 0). Molecular interactions inside the crystal are often approximated to be (screened) interactions between point-dipoles located at the centre of mass of each molecule and corresponding to the dipole moment of the molecular transition. Such an approximation fails for molecules close to each other compared to their dimensions and it can be improved by using the transition charge distribution method, which consists in

approximating the delocalized molecular transition dipole with a distribution of point charges located at atomic positions (Alessandrini et al. 2011, Markovitsi et al. 1995, Scholz et al. 2000, Vragovic & Scholz 2003). An even more accurate estimate of the molecular interactions can be obtained by quantum mechanical calculations involving several molecules, but such a refinement would be relevant only for nearest-neighbour or next-nearest-neighbour molecules and, in our test cases, would only slightly correct the absorption spectra. Particular care must be taken in computing the matrix elements $\tilde{J}_{\alpha\beta}(\mathbf{k})$, which, in the case of an infinite three-dimensional crystal, are non-analytic functions of $\mathbf{k}$ as $\mathbf{k}\rightarrow 0$. If molecules are approximated by point-dipoles it is possible to evaluate the infinite sum (2) using Ewald's method (Philpott & Lee 1973), which allows to isolate the non analytic term corresponding to long-range molecular interactions. It is therefore possible to calculate Coulomb or mechanical exciton states by including or neglecting long-range interactions. Ewald's method can also be applied in conjunction with the transition charge distribution method, because even in that case interactions between distant molecules are well approximated by interactions between point-dipoles. Once excitonic bands have been computed, it is possible to compute absorption spectra through the macroscopic dielectric tensor ε_{ij}. Since the wave vector of the incident light is usually much smaller than the reciprocal lattice cell size, absorption is due to excitonic states with $k\approx 0$, which also correspond to poles in the macroscopic dielectric tensor. The latter can be explicitly computed as a function of the incident light energy, $\hbar\omega$, as

$$\varepsilon_{ij}(\hbar\omega) = \varepsilon_{\infty}\delta_{ij} + \frac{2}{\varepsilon_0 V}\sum_n \frac{dn,i\ dn,j\ En}{E_n^2 - (\hbar\omega)^2 - i\gamma\hbar\omega} \tag{3}$$

where ε_{∞} is the high frequency dielectric constant, V is the unit cell volume, γ is a damping factor which determines the width of the absorption line shape, E_n is the energy of the nth mechanical exciton state at $k=0$ and $d_{n,i}$ is the ith component of its dipole moment. We point out that since mechanical excitons enter equation (3), the limit $k\rightarrow 0$ is well defined and does not depend on the direction of $\mathbf{k}$. Having the dielectric tensor, absorption and reflection spectra can be computed for a slab geometry by means of a transfer matrix method (Schubert 1996). In the case of more than one molecule per cell ($\sigma>1$) the Davydov splitting between excitonic bands at $k=0$ can be computed for each possible orientation of the crystal by simulating the absorption spectra of a very thin film. The above procedure splits the problem of computing absorption into two parts. First we compute the microscopic mechanical exciton states and then we consider the propagation of light in an anisotropic medium, including long-range interactions through the macroscopic dielectric tensor. This theoretical approach takes full account of all the crystal symmetries and the numerical calculations provide a fairly accurate description of the dispersion of the purely excitonic bands, allowing a quantitative comparison with experiments (Raimondo et al. 2006; Silvestri et al. 2009; Spearman et al. 2005; Tavazzi et al. 2006a, 2006b).

It is important to recognize that the properties of excitons in molecular crystals are strongly influenced by their coupling to intramolecular phonons, which give rise to the vibronic progressions typically observed in optical spectra. This is because in organic semiconductors electronic excitation is accompanied by significant nuclear rearrangements, which do not

occur in inorganic semiconductors instead. The conventional treatment of exciton-phonon coupling identifies different regimes by comparing the nuclear relaxation energy to a measure of the intermolecular (excitonic) interactions, usually taken to be the free-exciton bandwidth or, in the case of more than one molecule per unit cell, the free-exciton Davydov splitting *W*. For a single harmonic intramolecular vibrational mode of energy $\hbar\omega_v$, the nuclear relaxation energy is given by $\lambda^2\hbar\omega_v$, where λ^2 is the Huang–Rhys factor. Strong, intermediate and weak excitonic coupling corresponds to the three situations: $\lambda^2\hbar\omega_v << W$, $\lambda^2\hbar\omega_v \approx W$ and $\lambda^2\hbar\omega_v >> W$, respectively.

In the weak excitonic coupling regime, a good approximation is obtained by replacing free excitons with vibronic excitons (or vibrons), in which the electronic excitation and $\tilde{\mu}$ vibrational quanta reside on the same molecule. Such an approximation ignores higher particle states in which the deformation of the lattice surrounding the excitation allows for ground-state vibrations to coexist on neighbouring molecules (Philpott 1971, Spano 2003). In this regime, also called vibronic coupling regime, crystal eigenstates can be expressed in terms of delocalized vibronic states

$$\left|\mathbf{k},\alpha,\tilde{\mu}\right\rangle = N^{-1/2}\sum_{\mathbf{n}}\exp\left(i\mathbf{kn}\right)\left|\mathbf{n},\alpha,\tilde{\mu}\right\rangle,$$

where the additional quantum number $\tilde{\mu}$ indicates the number of vibrational quanta residing on molecule α in cell **n.** The corresponding vibrational Hamiltonian is

$$H_{vib} = \hbar\omega_0 + D + \sum_{\mathbf{k},\alpha,\tilde{\mu}}\tilde{\mu}\hbar\omega_v\left|\mathbf{k},\alpha,\tilde{\mu}\right\rangle\left\langle\mathbf{k},\alpha,\tilde{\mu}\right| + \sum_{\mathbf{k},\alpha,\beta,\tilde{\mu},\tilde{\nu}} S_{\tilde{\mu}0}S_{\tilde{\nu}0}\tilde{J}_{\alpha\beta}(\mathbf{k})\left|\mathbf{k},\alpha,\tilde{\mu}\right\rangle\left\langle\mathbf{k},\beta,\tilde{\nu}\right| \qquad (4)$$

where

$$S^2_{\tilde{\mu}0} = \exp\left(-\lambda^2\right)\lambda^{2\tilde{\mu}} / \tilde{\mu}!$$

are the Franck-Condon overlap factors. As it can be seen, in this coupling regime, the oscillator strength is redistributed among all the vibronic excitons with *k*=0 and each excitonic absorption line is replaced by a progression of vibronic replicas.

As the intermolecular coupling increases, the spectral centroid of each vibronic progression tends to shift and the Davydov splitting between different progressions increases. In the extreme case of strong excitonic coupling regime, all the oscillator strength of each progression is again concentrated in a single peak, corresponding to the free exciton state. There is essentially no nuclear relaxation subsequent to the electronic excitation because the excitation resonantly jumps to a neighbour before relaxation can occur. A more detailed description of the various exciton-phonon coupling regimes and of their spectral signatures in molecular aggregates can be found in the literature (Spano 2010).

3.2 TPB

TPB forms single crystals and can grow in at least three polymorphic forms (Baba et al. 2003; Girlando et al. 2010; Ino et al. 2000; Tavazzi et al. 2010b). The two most commonly obtained polymorphs have monoclinic structures known as α and β forms (Table 1). β-TPB is particularly interesting as it exhibits amplified spontaneous emission (ASE) from the widest crystal face (Tavazzi et al. 2010b). The essential crystallographic parameters of the two structures are reported in Table 1.

	α polymorph	β polymorph
Space group	$P2_1$	$P2_1/c$
a (Å)	6.259(2)	9.736(5)
b (Å)	22.164(4)	8.634(2)
c (Å)	7.362(3)	24.480(13)
α (deg)	90	90
β (deg)	96.349(4)	97.11(4)
γ (deg)	90	90
Z	2	4

Table 1. Crystal data for the α and β polymorphs of TPB (Girlando et al. 2010).

The electronic optical transitions of the isolated TPB molecule were calculated as reported elsewhere (Girlando et al. 2010; Tavazzi et al. 2010b). The lowest energy transition is found at about 3.6 eV for the conformations of both the α and the β polymorphs. In both cases, the lowest transition is by far the strongest one calculated in the interval 3-4.8 eV, and is strongly polarized along the longest inertial axis of the molecule (*L*), that is, along the butadiene skeleton, where the HOMO and LUMO are mostly localized. All the components of the transition dipole moment along the principal molecular axes *L*, *M*, *N* (where *M* and *N* are other inertial axes of the molecule, *N* being the shortest one) are reported in Table 2.

	α			β		
molecule	*L*	*M*	*N*	*L*	*M*	*N*
	-8.43	0.26	0.02	-8.22	0.73	0.12
crystals	*b*	*ac*		*b*	*ac*	
		a	*c**		*c*	*a**
	0	7.39	4.54	0	16.44	1.36
	8.19	0	0	0.50	0	0

Table 2. Components along the *L*, *M*, *N* molecular axes of the calculated dipole moments (Debyes) of the molecular electronic transition at lowest energy of α- and β- TPB and components along the unit-cell axes of the unit-cell excitonic transitions.

What is relevant is the relative orientation of the molecules within the crystal and especially with respect to the most developed crystal face to determine different UV-visible properties. The α polymorph has two molecules per unit cell, so that each molecular electronic transition gives rise to two excitonic bands. Both bands are optically allowed at **k**=0 (centre of the Brillouin zone). They are polarized in the *ac* plane and along the monoclinic *b* axis, respectively. For the molecular transition calculated at 3.6 eV, the projections of the unit-cell excitonic transition dipole moments at **k**=0 are reported in Table 2 with respect to the (*abc**) frame of reference (the most developed face of the crystals is typically along the *ac* plane). The two excitonic transitions have comparable intensities, and the direction of polarization of the *ac* component is predicted at 32° to the *a* axis. In β-TPB there are four molecules per unit cell, so that each molecular electronic transition gives rise to four excitonic bands. Only two of them are optically allowed, which are polarized in the *ac* plane and along the monoclinic *b* axis, respectively (Table 2). The most developed face of these crystals is typically along the *bc* plane. We notice that the *b* component of the β polymorph is negligible, so that the corresponding *ac* exciton takes almost the whole available oscillator strength. In particular, the latter is mostly polarized along *c*. Figure 9 summarises the

resonant splitting of the electronic transitions from the single molecule to the crystalline α or β polymorphs. The different way that the excitonic oscillator strength is distributed in the two polymorphs arises from the relative orientation of the butadiene skeleton between individual molecules in the two unit cells. In the α phase the butadiene backbones are arranged in a sort of herringbone structure, while in the β-phase the butadiene skeletons are parallel to each other and parallel to the *c* axis. As a result, one exciton dominates the UV-visible absorption spectrum and has twice the intensity of the corresponding α-transitions.

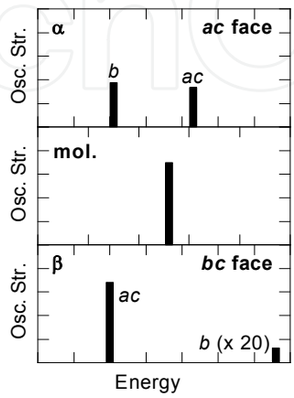

Fig. 9. Schematic picture of the modification of the first electronic transition of TPB from the isolated molecule (second panel) to the α and β crystals (first and third panels, where the labels indicate the polarization with respect to the unit-cell axes). The typical exposed face of the crystals of the two phases is also indicated.

The polarized absorption spectra of the exposed *ac* and *bc* crystal faces of α- and β-TPB, respectively, are reported in Fig. 10. The two continuous curves correspond to two orthogonal polarizations giving the maximum (//) and minimum (⊥) absorbance measured at normal incidence between 3 and 4 eV. The // spectrum saturates above about 3 eV. Despite the saturation, a band can be recognized. For the α polymorph, the maximum absorption at normal incidence is typically measured when the electric field of the incident light forms an angle of about 30° to one of the edges of the crystal. The comparison with the predicted value of 32° indicates that this edge corresponds to the *a* axis and the intense saturated band is attributed to the *ac* excitonic state of α-TPB. As expected, it becomes negligible in the ⊥ spectrum. For the β polymorph, the maximum absorption typically corresponds to one edge of the crystal. Indeed, the main peak can be attributed to the strong *ac* excitonic component, in particular to its *c* component (*bc* being the exposed face and the *c* axis lying along one edge of the crystal). At oblique incidence, another peak emerges centred at about 3.77 eV only for the α phase. It is attributed to the *b*-polarized excitonic component, which for this polymorph lies perpendicular to the exposed face. No emerging peaks were detected for the β phase, in agreement with the calculations which predict a negligible *b*-polarized component.

Up to now, we neglected possible effects due to vibronic coupling. The coupling of the electronic states with vibrational modes could induce shifts of the maxima of the optical bands resulting from a redistribution of the oscillator strength among the replicas. Fig. 11 shows the comparison between the simulated spectra (assuming weak excitonic coupling with one effective mode) for the polarization of the maximum absorption at normal incidence of the two polymorphs (i.e. at 32° to the *a* axis for the α polymorph and along the *c*

axis for the β polymorph). The replicas at lowest energies are favoured in the β phase, indicative of J-type i interaction, whilst the *ac*-polarized spectra of the α polymorph shows a

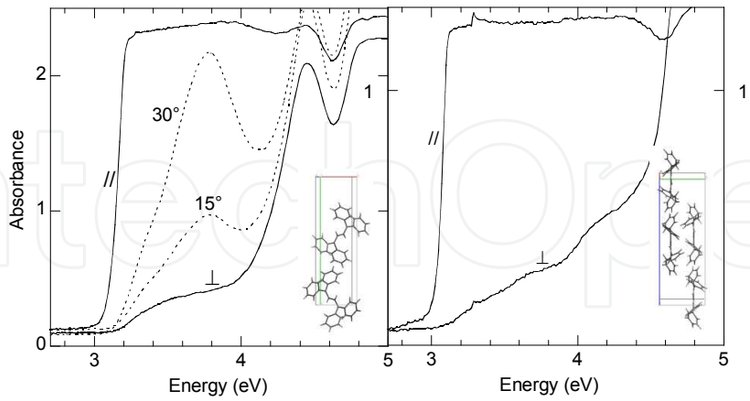

Fig. 10. Polarized absorbance spectra of monocrystals of α-TPB (left) and β-TPB monocrystals measured at normal incidence on the accessible face with two orthogonal polarizations corresponding to the minimum (⊥) and maximum (//) absorption between 3 and 4 eV and absorbance spectra (only for the α polymorph) taken at oblique incidence (angles of incidence 15° and 30°) with p-polarized light with plane of incidence defined by the direction of polarization of minimum absorption at normal incidence and the normal to the surface. Insets: sketch of the unit cell of the two polymorphs (left: α, right: β).

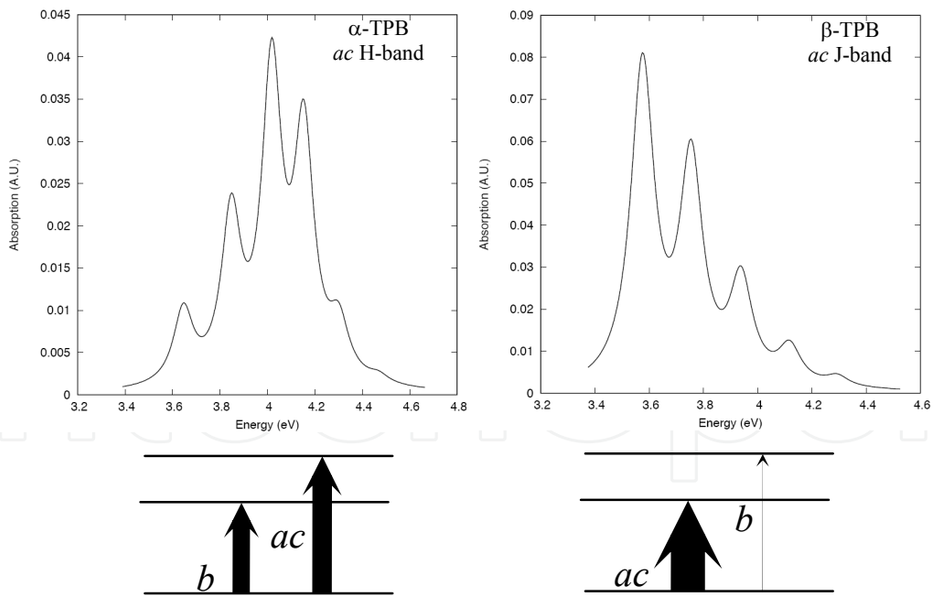

Fig. 11. Simulated absorbance spectra (vibronic approximation) corresponding to the polarization of the maximum absorption at normal incidence on the *ac* face of α-TPB (left) and on the *bc* face of β-TPB (right) (polarization direction at 30° to the *a* axis for the α polymorph and along the *c* axis for the β polymorph). The width of the arrows is proportional to the oscillator strength of the electronic transition.

shift of the maximum in absorption to higher energies due to the positive interaction energy for the upper transition, which is the one observed at normal incidence (H-type).
As far as the emission is concerned, the excitonic bands should be studied as a function of momentum $\boldsymbol{k}$ in the Brillouin zone. When the minimum of the excitonic band at the lowest energy is at k=0 or when the state at k=0 is thermally populated, the zero-phonon 0-0 emission transition is allowed and it is polarized as predicted by the excitonic model. For the α phase, the 0-0 emission transition is expected to be *b* polarized, in contrast to its vibronic replicas which are expected to be only partially polarized (Spano 2003, 2010). Since the crystals typically show the most developed face along the *ac* plane, the emitted light corresponding to the 0-0 transition is expected to be self-waveguided towards the borders, while at lower energy the emission from the replicas is expected both from the *ac* face and self-waveguided from the borders. For example, the image on the left of Fig. 3 was taken under the fluorescence microscope on a crystal with α crystal structure. In comparison, the 0-0 transition of the β polymorph is expected to be *ac* polarized, mainly along the *c* axis, which lies in the exposed *bc* face. Therefore, the 0-0 transition is expected to be detected when collecting the light from the face. The emission from the replicas is expected to be only partially polarized, but with much stronger intensity in the *c* polarization. Indeed, the molecular packing shown in the insets of Fig. 10 clearly indicates that in the β phase (and only in the β phase) the molecular transition moments (*L* polarized) are almost entirely parallel to the *c* axis (as also confirmed by the data in Table 2).

3.3 DBTDT

In order to circumvent the relatively low environmental stability of pentacene, heteroacenes, in which a carbocyclic ring or rings are replaced by a heteroaromatic group, have recently emerged (Anthony 2006, 2008; Bendikov et al. 2004; Gao et al. 2007; Gundlach et al. 1997; Jurchescu et al. 2004; Klauk et al. 2002; Li et al. 1998, Maliakal et al. 2004; Okamoto et al. 2005; Osuna et al. 2007; Sheraw et al. 2002; Wex et al. 2005; Xiao et al. 2005). DBTDT belongs to this family and here we use it to discuss an example of how the order of the electronic excited states changes due to intermolecular interactions. Okamoto and co-workers reported a UV-visible photophysical characterization and attribute the observed absorption bands of DBTDT to vibronic transitions of the single molecule (Okamoto et al. 2005). The electronic properties of the single DBTDT molecule and the structural properties in the solid state (Table 3) have been widely discussed also by Osuna et al., together with other thiophene- and selenophene-based heteroacenes studied by UV-visible-NIR spectroscopy (Osuna et al. 2007). The UV-visible absorption of a vacuum-deposited thin film of DBTDT has also been reported, which shows a characteristic red-shift of the lowest energy transition from solution to the solid state (Gao et al. 2007).

Space group	P*nma*
a (Å)	7.93
b (Å)	26.59
c (Å)	5.91
α (deg)	90
β (deg)	90
γ (deg)	90
Z	4

Table 3. Crystal data of DBTDT (Okamoto et al. 2005).

As discussed elsewhere (Alessandrini et al. 2011), the electronic optical transitions of the isolated molecule in vacuum and the corresponding directions of polarization were calculated using as input parameters the molecular geometries obtained from the crystallographic data. The components of the transition moments along the molecular axes (*L*, *M*, *N*, where *L* and *N* are the longest and shortest axes, respectively) are reported in Table 4 for the two lowest electronic transitions. The lowest energy band observed in solution (Okamoto et al. 2005; Osuna et al. 2007) is attributed to the transition calculated at lowest energy, which is also the strongest one. The calculated unit-cell dipole moments of the excitonic transitions at k=0 are also given in Table 4. Since the *L* molecular axes of all the four molecules in the unit cell are parallel to *b*, *L*-polarized molecular transitions give rise to a pure H aggregate and only one allowed *b*-polarized excitonic transition which is blue-shifted with respect to the molecular transition. By comparison, the molecular *M*-axes are organised in a herringbone fashion in the *ac* plane so that each *M*-polarized transition gives rise to two allowed excitonic transitions polarized along the *a* and *c* axes with significant projections along both of them.

molecule	*L*	*M*	*N*
	6.72	0	0
crystal	*a*	*b*	*c*
	0	13.44	0
molecule	*L*	*M*	*N*
	0	2.10	0
crystal	*a*	*b*	*c*
	1.93	0	3.73

Table 4. Components along the *L*, *M*, *N* molecular axes of the calculated dipole moments (Debyes) of the two molecular electronic transitions at lowest energy of DBTDT and components along the unit-cell axes of the corresponding excitonic transitions.

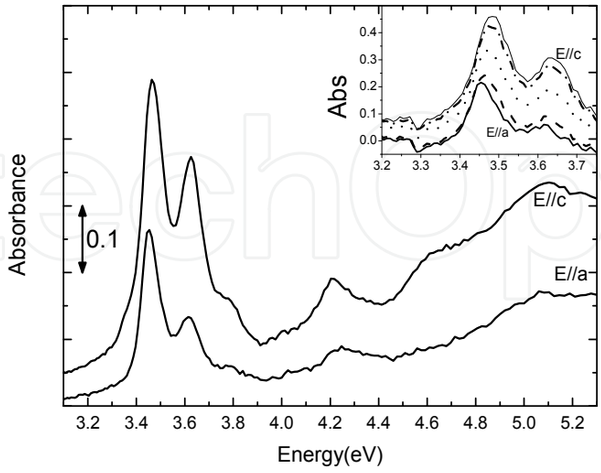

Fig. 12. Absorbance spectra of a DBTDT single crystal (50 nm thickness) taken at normal incidence with two orthogonal polarizations corresponding to the extremes high-energy shift (E//c) and low-energy shift (E//a) of the peaks between about 3.4 and 3.8 eV. Inset: spectra taken on the same crystal with intermediate polarizations.

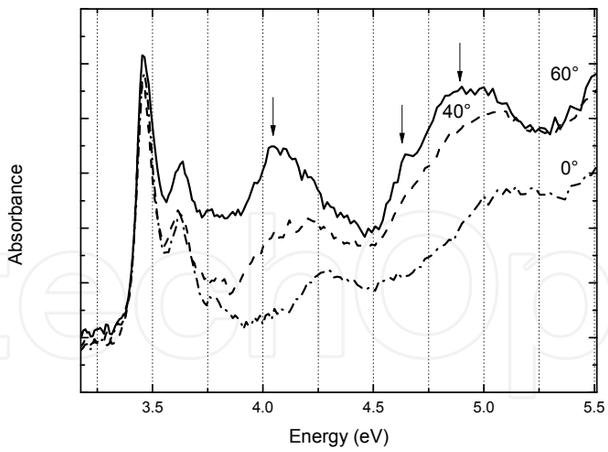

Fig. 13. Absorbance spectra of a DBTDT single crystal taken at different angles of incidence from 0° to 60° on the accessible face (*ac*) with *p* (*ab*) polarized light using the plane (*ab*) formed by the normal to the surface and the direction of polarization labelled as E//*a* in Fig. 12 as plane of incidence.

Polarized absorption spectra were taken at normal incidence to the most developed face of DBTDT crystals. Figure 12 shows the spectra of a monocrystal of about 50 nm in thickness. The reported spectra were measured with two orthogonal polarizations corresponding to the extremes of the low- and high-energy shift of the peaks between about 3.4 and 3.8 eV (the spectra taken with intermediate polarizations are shown in the inset in a restricted energy range). These two polarizations also correspond to the two directions of the electric field which give extinction of the transmitted light under crossed polarizer and analyzer. The spectra are dominated by two orthogonally-polarized vibronic series, with peaks at 3.45, 3.61 eV, and a shoulder at about 3.78 eV in one case, and at 3.46, 3.62 eV and a shoulder at about 3.78 eV in the other case. The stronger intensity is observed in the latter case. In Fig. 12, the two polarization directions are labelled E//a and E//c, since the comparison with the theoretical prediction (see below) allows deducing the corresponding polarization with respect to the axes of the crystal unit cell. Figure 13 shows the spectra taken at oblique incidence with p-polarized light (polarized in the plane of incidence) with plane of incidence formed by the normal to the surface and the direction of polarization labelled as E//a in Figure 12. Besides the replicas in the low-energy portion of the spectrum, at oblique incidence an emerging broad band is detected centred at about 4.07 eV, together with a further shoulder at about 4.6 eV and a structure at about 4.8 eV. The maximum intensity for these bands is detected for the highest angle of incidence; it decreases with decreasing angle of incidence, and eventually disappears at normal incidence.

The comparison between the experimental results and the theoretical predictions allows deducing that the accessible face, which is also the most developed one of the crystal, is the *ac* face. Indeed, two different excitonic transitions are detected in the normal incidence spectra, which are slightly shifted and orthogonally polarized. These bands are therefore attributed to the excitonic transitions (showing a vibronic progression) originating from the second *M*-polarized molecular electronic transition (calculated at 3.95 eV in this work and at 3.89 by Osuna et al. (Osuna et al. 2007). The labels E//*c* and E//*a* in Fig. 12 derive from this attribution. The Davydov splitting between the corresponding replicas of the *a* and *c*

progressions is about 0.01 eV. Such a low value indicates that, for this electronic transition, exciton coupling is relatively weak ($\lambda^2\hbar\omega_v >> W$). At higher energy in Fig. 12, broad and weaker bands are detected at about 4.21 and 5.07 eV, and 4.21 and 5.08 eV, for the two polarizations. These bands are attributed to other excitonic transitions in the *ac* plane of *M* molecular origin. The emerging band at 4.07 eV in oblique incidence spectra is attributed to the *b*-polarized excitonic transition originating from the strongest transition of the single molecule at the lowest energy. This molecular transition has been calculated at 3.86 eV in this work and at 3.77 eV by Osuna et al. (Osuna et al. 2007) and has been observed at about 3.6 eV in the solution spectra (Osuna et al. 2007; Okamoto et al. 2005). The blue-shift observed in the crystal spectra is explained by the arrangement of the corresponding *L*-molecular transition moments forming a pure H aggregate. We underline that polarized spectroscopy on monocrystals shows that there is no correspondence between the replicas observed at lowest energy in the solid state (originating from the second molecular transition) and the strong electronic transition at lowest energy of the single molecule. The diagram in Fig. 14 schematically shows the modification of the first and second electronic states from the single molecule to the crystal. Numerical calculations based on the method described in section 3.1 predicted, in the case of the first molecular transition, a Davydov splitting of 0.44 eV between the dark exciton at lowest energy and the allowed *b*-polarized upper exciton while, for the second molecular transition, the Davydov splitting between the two allowed excitons was found to be less than 0.01 eV, thus confirming the weak excitonic coupling of the second *M*-polarized molecular electronic transition. This suggests that the lowest excitonic transition (dark) coming from the first molecular transition is expected to be at about the same energy as the excitonic transitions detected in the normal-incidence spectra, which stems from the second molecular *M* transition.

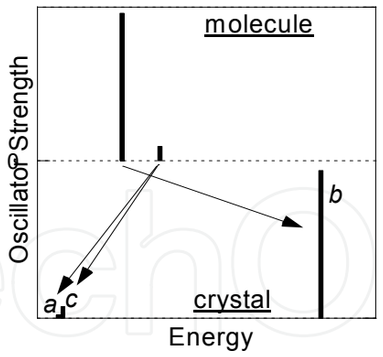

Fig. 14. Schematic picture of the modifications of the two lowest electronic transitions of DBTDT to the crystal excitons. The labels indicate the polarization of the excitonic states with respect to the unit-cell axes.

3.4 TPP

TPP is now taken into consideration to discuss another phenomenon, which may strongly influence the optical properties of molecular crystals, namely directional dispersion. Among thiophene/phenylene co-oligomers, this thiophene/phenyl co-oligomer end capped with pyrrole has been recently designed to explore the effect of an electron-rich aromatic ring, such as pyrrole, to end-cap oligothiophenes (Tavazzi et al. 2010a).

Space group	$P2_1$
a (Å)	5.77
b (Å)	7.43
c (Å)	24.72
α (deg)	90
β (deg)	91.76
γ (deg)	90
Z	2

Table 5. Crystal data for the α and β polymorphs of TPP (Tavazzi et al. 2010a).

The electronic optical transitions of the isolated molecule in vacuum were calculated (Tavazzi et al. 2010a) using as input parameters the molecular geometries obtained from the crystallographic data (Table 5). They were found at 2.95, 4.18, and 4.52 eV. In solution, the lowest absorption band was measured at about 3.1 eV (not shown here) and it is attributed to the lowest calculated transition. This transition is the strongest one with oscillator strength of 12.8 Debyes, which is quite high, compared to other conjugated molecules. For example, the lowest electronic transition of two of the most studied oligothiophenes, quaterthiophene and sexithiophene, have transition moments of about 10.6 and 10.4 Debyes, respectively (Petelenz & Andrzejak 2000; Silvestri et al. 2009; Spano et al. 2007). The components of the TPP transition at lowest energy with respect to the molecular inertial axes are listed in Table 6 and the results clearly indicate the strong polarization of the molecular transition at lowest energy along the long (*L*) molecular axis. In the crystal, each molecular electronic transition is predicted to give rise to two excitonic transitions, which are *b* and *ac* polarized. The components of the excitonic transitions were calculated and are provided in Table 6. There is a very weak *b* component and a strong *ac* component, mainly polarized along *c**, namely along the normal to the most developed face of the samples (the angle between the *ac* transition moment and the *c** axis is calculated to be about 7°). Indeed, the arrangement of the corresponding molecular transition moments in the unit cell gives rise to an almost pure H aggregate with almost parallel molecular transition moments.

Molecule	L	M	N
	-12.75	0.29	-0.10
crystal	*b*	*a*	*c**
	-0.18	0	0
	0	2.68	-17.84

Table 6. Components along the *L*, *M*, *N* molecular axes of the calculated dipole moment (in Debyes) of the molecular electronic transition at lowest energy of TPP and components along the unit-cell axes of the corresponding unit-cell excitonic transitions.

The measured absorption spectra taken in different configurations of a TPP single crystal are reported in Fig. 15. At normal incidence, the spectra correspond to two orthogonal polarizations giving the minimum and maximum absorption in the considered spectral range. These two polarizations also correspond to the two directions of the electric field which give extinction of the transmitted light under crossed polarizer and analyzer. The variable-angle measurements (at the angles of incidence indicated by the labels) were taken with *p* polarized light with plane of incidence formed by the normal to the surface and the

direction of polarization of the maximum absorption measured at normal incidence. The spectra are dominated by a main broad band. The intensity and shape of this band strongly depends on the angle of incidence. The maximum intensity is detected for the highest positive angle of incidence (the centre of the band can be tentatively deduced to be 3.75 eV), it decreases with decreasing angle of incidence down to zero at about -15°, and finally it again emerges slightly shifted at higher energy (the maximum is found at about 3.85 eV). This indicates that the corresponding transition moment has a strong component along the normal to the surface and shows directional dispersion (Philpott 1969; Spearman et al. 2005; Tavazzi et al. 2006b; Weiser & Moller 2002). Considering that the band disappears at about -15°, the inclination of the transition moment to the normal to the surface can be approximately estimated from the experiment to be of the order of -10° (taking into consideration the effect of refraction at the air/crystal interface).

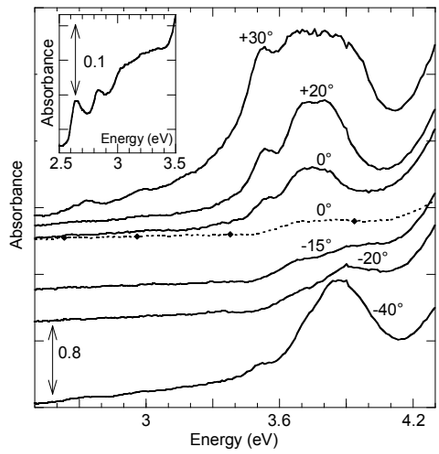

Fig. 15. Continuous lines: absorbance spectra of a TPP single crystal taken at different angles of incidence from +30° to -40° on the accessible face (*ab*) with *p*-polarized light and the plane formed by the normal to the surface and the direction of polarization of maximum absorption measured at normal incidence (*ac* plane) as plane of incidence. The portion of the spectrum between about 3.6 and 3.9 eV measured at +30° is affected by saturation. Dashed line with diamonds: normal-incidence spectrum with orthogonal (*b*) polarization). Inset: absorbance spectrum taken at normal incidence on a thicker crystal with *b* polarization.

The main band observed in Fig. 15 is attributed to the *ac* polarized exciton transition originating from the *L* molecular one, which is expected to be the strongest peak in the spectra. It reveals several structures (the lowest one at 2.73 eV, followed by shoulders at 2.97, 3.18 eV and by a peak centred at about 3.52 eV before the saturation region), which are easily detected for the highest angles of incidence and are attributed to vibronic replicas. The corresponding *b* excitonic component is not clearly observed in the spectra of Fig. 15, but it is recognizable in the spectrum (inset) taken in the same configuration on a thicker crystal with replicas of decreasing intensity at 2.65, 2.84, and 3.03 eV. On the basis of the calculated transition moments, the intensity ratio between the *ac* polarized and *b* polarized excitonic transitions is predicted to be of the order of 10^4. This ratio decreases for normal incidence spectra, where the intensity ratio between the *a*-component of the *ac* exciton and the *b* exciton is predicted to be about 200. Since the *ac* exciton transition dipole is nearly perpendicular to the *ab* plane, the

predicted ratio is only a rough estimate: a change as small as 1° degree in the molecular dipole inclination can produce a reduction of a factor 10 in the estimated intensity ratio. In any case, these low values explain the difficulty to detect the *b* excitonic transition for the thin sample whose spectra are shown in Fig. 15. The results of the optical characterization also indicate that the accessible face is the *ab* face (and the spectra in Fig. 15 were taken with *ac* as plane of incidence). Moreover, the *b* axis is a material principal axis and *ac* is a principal plane, thus explaining the extinction of the transmitted light under crossed polarizer and analyzer (Spearman et al. 2005). The energy difference between the lowest *b*-polarized peak (the most intense replica of the progression) and the centre of the *ac* polarized band measured at oblique incidence for positive angles is about 1.2 eV. Therefore, TPP satisfies the conditions of the strong excitonic coupling $\lambda^2\hbar\omega_v << W$: the *ac* exciton is almost free, it possesses nearly all the available oscillator strength and it is considerably blue-shifted with respect to the molecular electronic transition. The *ac* polarized replicas in the spectral region between 2.7 and 3.6 eV are built on the lower *b* polarized excitonic band and obtain their oscillator strength through an intermolecular Herzberg–Teller coupling to the nearly free *ac* polarized exciton (Silvestri et al. 2009; Spano 2003, 2004; Spano et al. 2007; Tavazzi et al. 2006a). On the contrary, the *b* polarized exciton is very weakly allowed and it is more strongly coupled to phonons, showing a vibronic progression. On the basis of the calculations and the measurements in solution, other excitonic transitions are expected originating from the higher molecular electronic transitions (Tavazzi et al. 2010a). Indeed, in the *b*-polarized normal-incidence spectrum, a relatively weak structure is also detected between about 3.4 and 4.0 eV, showing poorly defined replicas. A similar band cannot be excluded in the *a*-polarized spectrum below the *ac* exciton of *L* origin.

Figure 16 summarises the Davydov splitting of the electronic optical transition at lowest energy from the molecule to the crystal. The structural and optical characterization indicates that the crystals show an almost H-type aggregation of the electronic transition moment at lowest energy with strong excitonic coupling, giving rise to a large splitting of about 1.2 eV between an intense and almost free excitonic state polarized along the normal to the crystal surface and a weak *b*-polarized component. This large splitting results from the combination

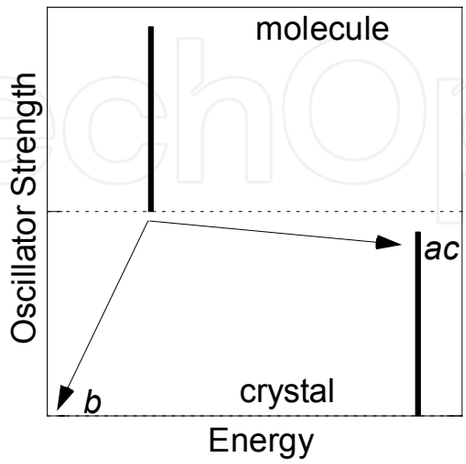

Fig. 16. Schematic representation of the Davydov splitting of the lowest electronic transition of TPP. The labels indicate the polarization of the excitonic states with respect to the unit-cell axes.

of the high oscillator strength and the steep inclination to the normal to the surface of the transition moment. Indeed, the splitting is demonstrated to be proportional to $(\hat{\mathbf{k}}_{inc}.\mathbf{d})^2$, where $\mathbf{k}_{inc}$ is the wave vector of the incoming light ($|\mathbf{k}_{inc}|\sim 0$) and $\mathbf{d}$ is the excitonic dipole moment (Philpott 1969; Spearman et al. 2005; Tavazzi et al. 2006b; Weiser & Moller 2002). Thus, TPP is an example with strong directional dispersion (energy and shape of the absorption band are strongly dependent on the angle of incidence on the crystal face).

4. Conclusion

In this chapter, we have reported some relevant effects on the optical properties of molecular solids related to the packing of the molecules in the crystal lattice using the general theory of molecular excitons. Three prototypical examples have been taken into consideration: (i) 1,1,4,4-tetraphenyl-1,3-butadiene (TPB), (ii) dibenzo[d,d′]thieno[3,2-b;4,5-b′]dithiophene (DBTDT), (iii) N-pyrrole end-capped thiophene/phenyl co-oligomer (TPP).

First of all, we have described few methods, which are often used for the crystal growth. The physical vapour growth requires a crucible for the starting material, a tube under inert-gas flow, and a furnace. An alternative method is the floating-drop technique, which requires two liquids, the molecule of interest being completely insoluble in one of them. The size of the grown crystals is typically relatively large. The third method that we have described is the melt growth, which is applicable when the molecular species possesses a well-defined melting point and remains stable at the corresponding temperature. Future opto-electronics device structures may exploit the crystalline form of molecular materials, but limiting factors are the control of their growth and device integration. A promising technique to overcome this barrier is to grow crystals from the melted compound, which can be incorporated into well-defined device geometries. As an example, we have shown the evolution during the TPP melt growth of the colour of the emission observed under a fluorescence microscope. The emission is green and isotropic when the compound is melted, but, upon decreasing the temperature, crystallization takes place and abruptly the green regions clearly show orange borders and dark exposed surface (with self-waveguiding of the emitted light).

The discussion of the UV-visible optical properties of molecular crystals is based on the Frenkel-Davydov exciton theory. First of all, we have mentioned a few important differences between organic and inorganic semiconductors in the framework of solid-state physics. The main differences are the different interaction energies among the molecules/atoms, the different energy dispersions of the electronic bands in the Brillouin zone as a function of momentum (and thus the different effective masses of the charge carriers), the formation of different types of excitons (either Frenkel-Davydov or Wannier-Mott), the differences in the packing of the constituent molecules/atoms, with possible strong optical anisotropy in the case of molecular solids, the different interactions of the respective excitons with vibrations/phonons. The Frenkel-Davydov theory underlines these aspects. It has been described and used to deduce the dielectric tensor of the three mentioned materials.

As far as TPB is concerned, it has been taken into consideration to discuss possible remarkable differences between polymorphs of the same molecular species. Indeed, a common consequence of different packing of the same molecular entity is polymorphism,

i.e. the occurrence of different crystalline phases. We have discussed that the different redistribution of the excitonic oscillator strength for the two polymorphs of TPB arises from the relative orientation of the butadiene skeleton between individual molecules in the two unit cells. In the α phase the butadiene backbones are arranged in a sort of herringbone structure, while in the β phase they are parallel to each other and almost parallel to one of the unit-cell axis. As a result, only one excitonic state dominates the UV-visible absorption spectrum, which has twice the intensity of the corresponding transitions in the α polymorph. These differences produce, in turn, differences in the exciton-vibration interaction. As discussed in the chapter, the coupling of the electronic states with vibrational modes can induce shifts of the maxima of the optical bands resulting from a redistribution of the oscillator strength among the replicas. For example, for TPB the replicas at lowest energies are favoured in the β phase (J-type interaction), while the normal-incidence spectra of the α polymorph shows a shift of the maximum in absorption to higher energies due to the positive interaction energy for the upper transition (H-type interaction).
DBTDT has been used as example to discuss the possible changes of the order of the excited states due to intermolecular interactions. The optical bands have been attributed to excitonic transitions showing a vibronic progression. However, there is no correspondence between the replicas observed at lowest energy in the solid state (originating from the second molecular transition) and the strong electronic transition at lowest energy of the molecule in solution (originating, as expected, from the first molecular transition). The remarkable blue-shift in the crystal of the first molecular transition is explained by the arrangement of the corresponding molecular transition moments forming a pure H aggregate.
Finally, TPP offers a prime example of the phenomenon of directional dispersion in which the molecular orientation within the crystal lattice affects the absorption spectra. This crystal shows an almost H-type aggregation of the electronic transition moment at lowest energy with strong excitonic coupling, giving rise to a large splitting at normal incidence of about 1.2 eV among the two allowed excitons. This large splitting results from the combination of the high oscillator strength of the molecular transition and the steep inclination to the normal to the surface of the transition moment since the splitting is proportional to the scalar product of the wave vector of the incoming light and the excitonic transition moment. Therefore, the energy and shape of the absorption band are strongly dependent on the angle of incidence on the exposed crystal face.
The chapter is mainly focused on the UV-visible absorption properties. A full description of the polarized emission spectra of molecular crystals requires the study of the excitonic bands in the whole first Brillouin zone (not only at the center of the Brillouin zone as for the interpretation of the absorption properties). However, some discussion on the emission properties has been given. For example, we have mentioned which are the expected directions and polarizations of either the zero-phonon emission transition or its replicas. We underline that future device structures may exploit the crystalline forms of molecular solids to provide highly directional emission useful in laser applications (vertical surface emitting geometries) or edge emission.

5. Acknowledgment

Fondazione Cariplo is acknowledged for financial support.

6. References

Adachi, H., Takano, K., Morikawa, M., Kanaya, S., Yoshimura, M., Mori, Y. & Sasaki, T. (2003) 'Application of a two-liquid system to sitting-drop vapour-diffusion protein crystallization', *Acta Crystallographica Section D-Biological Crystallography,* 59, 194-196.

Alessandrini, L., Braga, D., Jaafari, A., Miozzo, L., Mora, S., Silvestri, L., Tavazzi, S. & Yassar, A. (2011) 'Optical Properties of Dibenzo d,d ' thieno 3,2-b;4,5-b ' dithiophene Monocrystals: The Effect of Intermolecular Interactions', *Journal of Physical Chemistry A,* 115(3), 225-231.

Anthony, J. E. (2006) 'Functionalized Acenes and Heteroacenes for Organic Electronics', *Chemical Reviews,* 106(12), 5028-5048.

Anthony, J. E. (2008) 'The larger acenes: Versatile organic semiconductors', *Angewandte Chemie-International Edition,* 47(3), 452-483.

Baba, K., Kasai, H., Okada, S., Oikawa, H. & Nakanishi, H. (2003) 'Fabrication of organic nanocrystals using microwave irradiation and their optical properties', *Optical Materials,* 21(1-3), 591-594.

Bendikov, M., Wudl, F. & Perepichka, D. F. (2004) 'Tetrathiafulvalenes, oligoacenenes, and their buckminsterfullerene derivatives: The brick and mortar of organic electronics', *Chemical Reviews,* 104(11), 4891-4945.

Campione, M., Ruggerone, R., Tavazzi, S. & Moret, M. (2005) 'Growth and characterisation of centimetre-sized single crystals of molecular organic materials', *Journal of Materials Chemistry,* 15(25), 2437-2443.

Cordella, F., Quochi, F., Saba, M., Andreev, A., Sitter, H., Sariciftci, N. S., Mura, A. & Bongiovanni, G. (2007) 'Optical gain performance of epitaxially grown para-sexiphenyl films', *Advanced Materials,* 19(17), 2252.

Fichou, D., Delysse, S. & Nunzi, J. M. (1997) 'First evidence of stimulated emission from a monolithic organic single crystal: alpha-octithiophene', *Advanced Materials,* 9(15), 1178.

Fichou, D., Dumarcher, V. & Nunzi, J. M. (1999) 'One- and two-photon stimulated emission in oligothiophenes single crystals', *Optical Materials,* 12(2-3), 255-259.

Frolov, S. V., Vardeny, Z. V. & Yoshino, K. (1998) 'Cooperative and stimulated emission in poly(p-phenylene-vinylene) thin films and solutions', *Physical Review B,* 57(15), 9141-9147.

Gao, J., Li, R., Li, L., Meng, Q., Jiang, H., Li, H. & Hu, W. (2007) 'High-performance field-effect transistor based on dibenzo[d,d']thieno[3,2-b;4,5-b']dithiophene, an easily synthesized semiconductor with high ionization potential', *Adv. Mater. (Weinheim, Ger.),* 19, 3008-3011.

Girlando, A., Ianelli, S., Bilotti, I., Brillante, A., Della Valle, R. G., Venuti, E., Campione, M., Mora, S., Silvestri, L., Spearman, P. & Tavazzi, S. (2010) 'Spectroscopic and Structural Characterization of Two Polymorphs of 1,1,4,4-Tetraphenyl-1,3-butadiene', *Crystal Growth & Design,* 10(6), 2752-2758.

Gundlach, D. J., Lin, Y. Y., Jackson, T. N., Nelson, S. F. & Schlom, D. G. (1997) 'Pentacene organic thin-film transistors - molecular ordering and mobility', *IEEE Electron Device Lett.,* 18, 87-89.

Hibino, R., Nagawa, M., Hotta, S., Ichikawa, M., Koyama, T. & Taniguchi, Y. (2002) 'Emission gain-narrowing from melt-recrystallized organic semiconductor', *Advanced Materials,* 14(2), 119.

Hiramatsu, T., Matsuoka, N., Yanagi, H., Sasaki, F. & Hotta, S. (2009) 'Gain-narrowed emissions of thiophene/phenylene co-oligomer single crystals', *Physica Status Solidi C,* 6(1), 338.

Horowitz, G., Kouki, F., El Kassmi, A., Valat, P., Wintgens, V. & Garnier, F. (1999) 'Structure-dependent fluorescence in sexithiophene single crystals', *Advanced Materials,* 11(3), 234.

Ichikawa, M., Hibino, R., Inoue, M., Haritani, T., Hotta, S., Araki, K., Koyama, T. & Taniguchi, Y. (2005) 'Laser oscillation in monolithic molecular single crystals', *Advanced Materials,* 17(17), 2073.

Ichikawa, M., Hibino, R., Inoue, M., Haritani, T., Hotta, S., Koyama, T. & Taniguchi, Y. (2003) 'Improved crystal-growth and emission gain-narrowing of thiophene/phenylene co-oligomers', *Advanced Materials,* 15(3), 213.

Ino, I., Wu, L. P., Munakata, M., Kuroda-Sowa, T., Maekawa, M., Suenaga, Y. & Sakai, R. (2000) 'Bridged silver(I) complexes of the polycyclic aromatic compounds tetraphenylethylene and 1,1,4,4-tetraphenyl-1,3-butadiene', *Inorganic Chemistry,* 39(24), 5430-5436.

Jurchescu, O. D., Baas, J. & Palstra, T. T. M. (2004) 'Effect of impurities on the mobility of single crystal pentacene', *Applied Physics Letters,* 84(16), 3061-3063.

Kena-Cohen, S., Davanco, M. & Forrest, S. R. (2008) 'Strong exciton-photon coupling in an organic single crystal microcavity', *Physical Review Letters,* 101(11), 116401.

Kena-Cohen, S. & Forrest, S.R. (2010) 'Room-temperature polariton lasing in an organic single-crystal microcavity', *Nature Photonics*, 4, 371.

Klaers, J., Schmitt, J., Vewinger, F. & Weitz, M. (2010) 'Bose-Einstein condensation of photons in an optical microcavity', *Nature,* 468(7323), 545-548.

Klauk, H., Halik, M., Zschieschang, U., Schmid, G., Radlik, W. & Weber, W. (2002) 'High-mobility polymer gate dielectric pentacene thin film transistors', *Journal of Applied Physics,* 92(9), 5259-5263.

Kloc, C. & Laudise, R. A. (1998) 'Vapor pressures of organic semiconductors: α-hexathiophene and α-quaterthiophene', *J. Cryst. Growth,* 193, 563-571.

Kloc, C., Simpkins, P. G., Siegrist, T. & Laudise, R. A. (1997) 'Physical vapor growth of centimeter-sized crystals of α-hexathiophene', *J. Cryst. Growth,* 182, 416-427.

Kondo, H., Tongu, K., Yamamoto, Y., Yamamoto, S. & Kurisu, H. (2009) 'Cavity polariton dispersion of a single-crystalline anthracene film embedded in a microcavity', *Phys. Status Solidi C,* 6, 284-287.

Kondo, H., Yamamoto, Y., Takeda, A., Yamamoto, S. & Kurisu, H. (2008) 'Optical responses in single-crystalline organic microcavities', *J. Lumin.,* 128, 777-779.

Laudise, R. A., Kloc, C., Simpkins, P. G. & Siegrist, T. (1998) 'Physical vapor growth of organic semiconductors', *J. Cryst. Growth,* 187, 449-454.

Li, X. C., Sirringhaus, H., Garnier, F., Holmes, A. B., Moratti, S. C., Feeder, N., Clegg, W., Teat, S. J. & Friend, R. H. (1998) 'A highly pi-stacked organic semiconductor for thin film transistors based on fused thiophenes', *Journal of the American Chemical Society,* 120(9), 2206-2207.

Liu, C. Y. & Bard, A. J. (2000) 'In-situ regrowth and purification by zone melting of organic single-crystal thin films yielding significantly enhanced optoelectronic properties', *Chemistry of Materials,* 12(8), 2353-2362.

Losio, P. A., Hunziker, C. & Guenter, P. (2007) 'Amplified spontaneous emission in para-sexiphenyl bulk single crystals', *Applied Physics Letters,* 90(24), 241103.

Maliakal, A., Raghavachari, K., Katz, H., Chandross, E. & Siegrist, T. (2004) 'Photochemical stability of pentacene and a substituted pentacene in solution and in thin films', *Chemistry of Materials,* 16(24), 4980-4986.

Markovitsi, D., Germain, A., Millie, P., Lecuyer, P., Gallos, L., Argyrakis, P., Bengs, H. & Ringsdorf, H. (1995) 'Triphenylene Columnar Liquid Crystals: Excited States and Energy Transfer', *J. Phys. Chem.,* 99, 1005-17.

Matsuoka, N., Hiramatsu, T., Yanagi, H., Sasaki, F. & Hotta, S. (2010) 'Characterization of Gain-Narrowed Emission from Biphenyl-Capped Thiophene Single Crystals', *Japanese Journal of Applied Physics,* 49(1), 01AD05.

Meinardi, F., Borghesi, A., Cerminara, M., Sassella, A., Tavazzi, S., Tubino, R., Gurioli, M., Mura, A. & Bongiovanni, G. (2001) 'The origin of radiative emission of quaterthiophene ultra-thin films', *Synth. Met.,* 121, 1355-1356.

Nagawa, M., Hibino, R., Hotta, S., Yanagi, H., Ichikawa, M., Koyama, T. & Taniguchi, Y. (2002) 'Emission gain narrowing from single crystals of a thiophene/phenylene co-oligomer', *Applied Physics Letters,* 80(4), 544-546.

Okamoto, T., Kudoh, K., Wakamiya, A. & Yamaguchi, S. (2005) 'General synthesis of thiophene and selenophene-based heteroacenes', *Organic Letters,* 7(23), 5301-5304.

Osuna, R. M., Ponce Ortiz, R., Okamoto, T., Suzuki, Y., Yamaguchi, S., Hernandez, V. & Lopez Navarrete, J. T. (2007) 'Thiophene- and selenophene-based heteroacenes: Combined quantum chemical DFT and spectroscopic Raman and UV-vis-NIR study', *Journal of Physical Chemistry B,* 111(26), 7488-7496.

Park, S., Kwon, O. H., Kim, S., Choi, M. G., Cha, M., Park, S. Y. & Jang, D. J. (2005) 'Imidazole-based excited-state intramolecular proton-transfer materials: Synthesis and amplified spontaneous emission from a large single crystal', *Journal of the American Chemical Society,* 127(28), 10070-10074.

Petelenz, P. & Andrzejak, M. (2000) 'Vibronic interpretation of the low-energy absorption spectrum of the sexithiophene single crystal', *Journal of Chemical Physics,* 113(24), 11306-11314.

Philpott, M. R. (1969) 'Dipole Davydov splittings in crystalline anthracene, tetracene, naphthalene, and phenanthrene', *J. Chem. Phys.,* 50, 5117-28.

Philpott, M. R. (1971) 'Theory of coupling of electronic and vibrational excitations in molecular crystals and helical polymers', *Journal of Chemical Physics,* 55(5), 2039.

Philpott, M. R. & Lee, J. W. (1973) 'Some remarks on calculation and use of retarded and static dipole sums in molecular exciton theory', *Journal of Chemical Physics,* 58(2), 595-602.

Polo, M., Camposeo, A., Tavazzi, S., Raimondo, L., Spearman, P., Papagni, A., Cingolani, R. & Pisignano, D. (2008) 'Amplified spontaneous emission in quaterthiophene single crystals', *Applied Physics Letters,* 92(8), 083311.

Quochi, F., Cordella, F., Mura, A., Bongiovanni, G., Balzer, F. & Rubahn, H. G. (2005) 'One-dimensional random lasing in a single organic nanofiber', *Journal of Physical Chemistry B,* 109(46), 21690-21693.

Raimondo, L., Campione, M., Laicini, M., Moret, M., Sassella, A., Spearman, P. & Tavazzi, S. (2006) 'Absorbance spectra of polycrystalline samples and twinned crystals of oligothiophenes', *Appl. Surf. Sci.,* 253, 271-274.

Scholz, R., Kobitski, A. Y., Kampen, T. U., Schreiber, M., Zahn, D. R. T., Jungnickel, G., Elstner, M., Sternberg, M. & Frauenheim, T. (2000) 'Resonant Raman spectroscopy of 3,4,9,10-perylene-tetracarboxylic-dianhydride epitaxial films', *Physical Review B,* 61(20), 13659-13669.

Schubert, M. (1996) 'Polarization-dependent optical parameters of arbitrarily anisotropic homogeneous layered systems', *Phys. Rev. B: Condens. Matter,* 53, 4265-74.

Sheraw, C. D., Zhou, L., Huang, J. R., Gundlach, D. J., Jackson, T. N., Kane, M. G., Hill, I. G., Hammond, M. S., Campi, J., Greening, B. K., Francl, J. & West, J. (2002) 'Organic thin-film transistor-driven polymer-dispersed liquid crystal displays on flexible polymeric substrates', *Appl. Phys. Lett.,* 80, 1088-1090.

Siegrist, T., Kloc, C., Laudise, R. A., Katz, H. E. & Haddon, R. C. (1998) 'Crystal growth, structure, and electronic band structure of α-4T polymorphs', *Adv. Mater. (Weinheim, Ger.),* 10, 379-382.

Silvestri, L., Tavazzi, S., Spearman, P., Raimondo, L. & Spano, F. C. (2009) 'Exciton-phonon coupling in molecular crystals: Synergy between two intramolecular vibrational modes in quaterthiophene single crystals', *Journal of Chemical Physics,* 130(23), 234701.

Spano, F. C. (2003) 'The fundamental photophysics of conjugated oligomer herringbone aggregates', *J. Chem. Phys.,* 118, 981-994.

Spano, F. C. (2004) 'Temperature dependent exciton emission from herringbone aggregates of conjugated oligomers', *J. Chem. Phys.,* 120, 7643-7658.

Spano, F. C. (2010) 'The Spectral Signatures of Frenkel Polarons in H- and J-Aggregates', *Acc. Chem. Res.,* 43, 429-439.

Spano, F. C., Silvestri, L., Spearman, P., Raimondo, L. & Tavazzi, S. (2007) 'Reclassifying exciton-phonon coupling in molecular aggregates: Evidence of strong nonadiabatic coupling in oligothiophene crystals', *Journal of Chemical Physics,* 127(18), 184703.

Spearman, P., Borghesi, A., Campione, M., Laicini, M., Moret, M. & Tavazzi, S. (2005) 'Directional dispersion in absorbance spectra of oligothiophene crystals', *J. Chem. Phys.,* 122, 014706/1-014706/6.

Tavazzi, S., Borghesi, A., Gurioli, M., Meinardi, F., Riva, D., Sassella, A., Tubino, R. & Garnier, F. (2003) 'Absorption and emission properties of α,ω-dihexyl-quaterthiophene thin films grown by organic molecular beam deposition', *Synth. Met.,* 138, 55-58.

Tavazzi, S., Borghesi, A., Papagni, A., Spearman, P., Silvestri, L., Yassar, A., Camposeo, A., Polo, M. & Pisignano, D. (2007) 'Optical response and emission waveguiding in rubrene crystals', *Physical Review B,* 75(24), 245416.

Tavazzi, S., Campione, M., Laicini, M., Raimondo, L., Borghesi, A. & Spearman, P. (2006a) 'Measured Davydov splitting in oligothiophene crystals', *J. Chem. Phys.,* 124, 194710/1-194710/7.

Tavazzi, S., Laicini, M., Raimondo, L., Spearman, P., Borghesi, A., Papagni, A. & Trabattoni, S. (2006b) 'Evidence of polarized charge-transfer transitions by probing the weak dielectric tensor components of oligothiophene crystals', *Appl. Surf. Sci.,* 253, 296-299.

Tavazzi, S., Miozzo, L., Silvestri, L., Mora, S., Spearman, P., Moret, M., Rizzato, S., Braga, D., Diaw, A. K. D., Gningue-Sall, D., Aaron, J.-J. & Yassar, A. (2010a) 'Crystal Structure and Optical Properties of N-Pyrrole End-Capped Thiophene/Phenyl Co-Oligomer: Strong H-type Excitonic Coupling and Emission Self-Waveguiding', *Crystal Growth & Design,* 10(5), 2342-2349.

Tavazzi, S., Raimondo, L., Silvestri, L., Spearman, P., Camposeo, A., Polo, M. & Pisignano, D. (2008) 'Dielectric tensor of tetracene single crystals: The effect of anisotropy on polarized absorption and emission spectra', *Journal of Chemical Physics,* 128(15), 154709.

Tavazzi, S., Silvestri, L., Miozzo, L., Papagni, A., Spearman, P., Ianelli, S., Girlando, A., Camposeo, A., Polo, M. & Pisignano, D. (2010b) 'Polarized Absorption, Spontaneous and Stimulated Blue Light Emission of J-type Tetraphenylbutadiene Monocrystals', *Chemphyschem,* 11(2), 429-434.

Tavazzi, S., Spearman, P., Silvestri, L., Raimondo, L., Camposeo, A. & Pisignano, D. (2006c) 'Propagation properties and self-waveguided fluorescence emission in conjugated molecular solids', *Organic Electronics,* 7(6), 561-567.

Vragovic, I. & Scholz, R. (2003) 'Frenkel exciton model of optical absorption and photoluminescence in alpha-PTCDA', *Physical Review B,* 68(15).

Weiser, G. & Moller, S. (2002) 'Directional dispersion of the optical resonance of pi-pi* transitions of alpha-sexithiophene single crystals', *Physical Review B,* 64(5), 045203.

Wex, B., Kaafarani, B. R., Kirschbaum, K. & Neckers, D. C. (2005) 'Synthesis of the anti and syn Isomers of Thieno[f,f']bis[1]benzothiophene. Comparison of the Optical and Electrochemical Properties of the anti and syn Isomers', *J. Org. Chem.,* 70, 4502-4505.

Xiao, K., Liu, Y. Q., Qi, T., Zhang, W., Wang, F., Gao, J. H., Qiu, W. F., Ma, Y. Q., Cui, G. L., Chen, S. Y., Zhan, X. W., Yu, G., Qin, J. G., Hu, W. P. & Zhu, D. B. (2005) 'A highly pi-stacked organic semiconductor for field-effect transistors based on linearly condensed pentathienoacene', *Journal of the American Chemical Society,* 127(38), 13281-13286.

Xie, W., Li, Y., Li, F., Shen, F. & Ma, Y. (2007) 'Amplified spontaneous emission from cyano substituted oligo(p-phenylene vinylene) single crystal with very high photoluminescent efficiency', *Applied Physics Letters,* 90(14), 141110.

Yanagi, H. & Morikawa, T. (1999) 'Self-waveguided blue light emission in p-sexiphenyl crystals epitaxially grown by mask-shadowing vapor deposition', *Applied Physics Letters,* 75(2), 187-189.

Yanagi, H., Ohara, T. & Morikawa, T. (2001) 'Self-waveguided gain-narrowing of blue light emission from epitaxially oriented p-sexiphenyl crystals', *Advanced Materials,* 13(19), 1452.

Zhu, X. H., Gindre, D., Mercier, N., Frere, P. & Nunzi, J. M. (2003) 'Stimulated emission from a needle-like single crystal of an end-capped fluorene/phenylene co-oligomer', *Advanced Materials,* 15(11), 906.

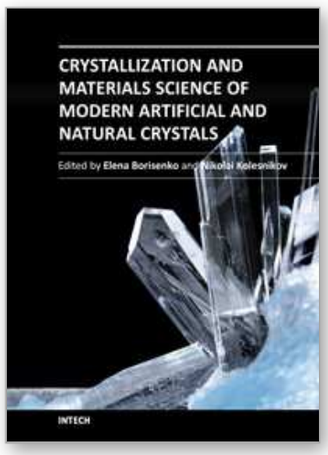

Crystallization and Materials Science of Modern Artificial and Natural Crystals

Edited by Dr. Elena Borisenko

ISBN 978-953-307-608-9
Hard cover, 328 pages
Publisher InTech
Published online 20, January, 2012
Published in print edition January, 2012

Crystal growth is an important process, which forms the basis for a wide variety of natural phenomena and engineering developments. This book provides a unique opportunity for a reader to gain knowledge about various aspects of crystal growth from advanced inorganic materials to inorganic/organic composites, it unravels some problems of molecular crystallizations and shows advances in growth of pharmaceutical crystals, it tells about biomineralization of mollusks and cryoprotection of living cells, it gives a chance to learn about statistics of chiral asymmetry in crystal structure.

InTech Europe
University Campus STeP Ri
Slavka Krautzeka 83/A
51000 Rijeka, Croatia
Phone: +385 (51) 770 447
Fax: +385 (51) 686 166
www.intechopen.com

InTech China
Unit 405, Office Block, Hotel Equatorial Shanghai
No.65, Yan An Road (West), Shanghai, 200040, China
中国上海市延安西路65号上海国际贵都大饭店办公楼405单元
Phone: +86-21-62489820
Fax: +86-21-62489821

IntechOpen